Computers and Concrete, *Vol. 23, No. 1 (2019) 25-36*
DOI: https://doi.org/10.12989/cac.2019.23.1.025

An algorithm for simulation of cyclic eccentrically-loaded RC columns using fixed rectangular finite elements discretization

Kabir Sadeghi* and Fatemeh Nouban[a]

Civil and Environmental Engineering Faculty, Near East University, Near East Boulevard, ZIP: 99138, Nicosia, North Cyprus, via Mersin 10, Turkey

(Received November 5, 2018, Revised January 20, 2019, Accepted January 22, 2018)

Abstract. In this paper, an algorithm is presented to simulate numerically the reinforced concrete (RC) columns having any geometric form of section, loaded eccentrically along one or two axes. To apply the algorithm, the columns are discretized into two macro-elements (MEs) globally and the critical sections of columns are discretized into fixed rectangular finite elements locally. A proposed triple simultaneous dichotomy convergence method is applied to find the equilibrium state in the critical section of the column considering the three strains at three corners of the critical section as the main characteristic variables. Based on the proposed algorithm a computer program has been developed for simulation of the nonlinear behavior of the eccentrically-loaded columns. A good agreement has been witnessed between the results obtained applying the proposed algorithm and the experimental test results. The simulated results indicate that the ultimate strength and stiffness of the RC columns increase with the increase in axial force value, but large axial loads reduce the ductility of the column, make it brittle, impose great loss of material, and cause early failure.

Keywords: reinforced concrete; columns; simulation; monotonic; cyclic; eccentrically-loaded

1. Introduction

The behavior of eccentrically-loaded RC columns has been investigated by several researchers. Among them, Szerszen *et al*. (2005) presented a reliability analysis for eccentrically-loaded RC columns. The strength limit state functions were developed for rectangular section RC columns, depending on the cross-section dimension, reinforcement percentage, and load eccentricity condition. For each given eccentricity state, the axial force-bending moment interaction diagram was developed. The statistical parameters of resistance were calculated employing the Monte Carlo simulation method. Amziane and Dubé (2008) have proposed an algorithm to simulate RC structures subjected to the axial load combined with the cyclic uniaxial bending. Pires and Silva (2014) presented a numerical processing model to analyze RC columns under axial loads and bending moment. They used a finite element method for calculating displacements. Their proposed model is applicable only to rectangular cross-sectional columns. Elwan and Omar (2014) examined the behavior of slender RC columns under eccentric loads. They compared the obtained results with the result got from the columns confined with external glass fiber reinforced polymers (GFRP) sheets. The monodirectional eccentricity ratios (*e/t*) of 0, 0.10, and 0.50 were tested in each column with a slenderness ratio of 20. The obtained results indicated that the GFRP confining arrangement can be useful, particularly for the slender columns with small eccentricities. Nigdeli *et al*. (2015) proposed an optimization method in the analysis of the biaxially-loaded RC columns. They proposed a new computation approach applying an iterative analysis in several stages. In their proposed approach they combined the random iterations with music inspired metaheuristic algorithm entitled “harmony search”. They concluded that the proposed technique is useful to optimize the result obtained for a column having a different number of bars and different sizes of the column. Rodrigues *et al*. (2015) proposed a numerical model for simulation of the failure of slender RC columns under the eccentric axial forces. In this model, the responses of the concrete under tension and compression are defined by two scalar damage variables that present two different damage surfaces to control the dimension of the elastic domain. To model the behavior of the reinforcing steel bars, the elastic-plastic material model was applied. Massumi and Badkoubeh (2015) submitted a numerical method to provide the ultimate moment and related curvature values for the circular and rectangular cross-sections of the RC columns under axial loading and biaxial bending. A dimensionless formula applicable to the columns having the sections with similar mechanical properties and geometry has been proposed by them. Shirmohammadi and Esmaeily (2016) developed a computer application to analyze the performance of RC columns under different types of loading cases such as non-sequential axial force and cyclic biaxial load or displacement. The application can be applied to test the analytical models employing proper experimental test data. Abd El Fattah *et al*. (2017) developed a partial confinement

*Corresponding author, Professor
E-mail: kabir.sadeghi@neu.edu.tr
[a]Assistant Professor
E-mail: fatemeh.nouban@neu.edu.tr

ISSN: 1598-8198 (Print), 1598-818X (Online)

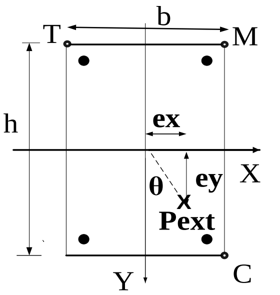

Fig. 1 Applied eccentric axial load on a column's section

model for rectangular RC column sections subjected to general eccentric loading. The model realizes an inverse correlation between the compression zone to the entire section ratio and the eccentricity of the axial compression force due to biaxial moment resultant. The procedure successfully predicted the confined capacity of rectangular RC columns. The partial confinement effects were shown to be significant or negligible based on the level of transverse steel confinement in the section. Peng and Guner (2018) modeled five RC frames employing a finite element analysis technique to illustrate the accuracy of pushover analyses for the seismically-deficient frames. Based on a developed computer program for the direct displacement-based design (D-DBD) procedure, they simulated the load capacities, story drifts, as well as the failure modes of the frames.

Kang and Lee (2018) studied the damage index values calculated from nonlinear finite element analysis of an RC column under cyclic loading and proposed a correction method. The modified damage index values were submitted in the quasi-static cyclic simulation.

To calculate the RC columns' sections subjected to the cyclic eccentric loading (CEL), the direct search method is employed to find the strain equilibrium plane. In this case, the section is discretized into fixed rectangular finite elements (FRFEs). This technique can be employed in both monotonic and cyclic loading cases.

In this paper, an algorithm to simulate numerically the nonlinear behavior of cyclic eccentrically-loaded RC columns (see Fig. 1) is proposed. To simulate the RC columns under cyclic loading, the FRFEs discretization type is adapted to discretize the critical sections.

In the proposed algorithm the nonlinear constitutive laws adapted to the nonlinear behavior of the confined and unconfined concretes and reinforcing steel are employed that can model the concrete cover loss and the confined concrete elements' failure. The instantaneous strengths of the columns along with detailed information are calculated at any stage of loading up to the failure of the columns. The proposed algorithm allows the user to overcome the divergence issue at inflection points and peak loading when calculating the column's response. By applying the proposed triple simultaneous dichotomy convergence search method, the convergence is guaranteed for any loading case.

2. Summary of the developed computer program

A computer program called "RC columns' analysis program" (RCCAP) has been developed by the authors to simulate the response of RC columns subjected to cyclic combined loading including eccentric axial force and inclined lateral loading. The main sub-programs of RCCAP are: CELS (combined eccentric loading simulation), CS (concrete simulation including confined and unconfined concretes simulation), RS (reinforcement simulation), NALS (neutral axis location simulation), DS (displacement simulation), BM-AL ID (bending moment-axial load interaction diagram), DRSFS (damping ratio and stiffness factor simulation) and DIS (damage index simulation).

RCCAP is capable of simulating the internal local behavior of the columns' critical sections (strain and stress in concrete and steel elements, neutral axis location, material loss and local damage (Sadeghi and Nouban 2017) and the overall behavior of the column (displacement, curvature, damping ratio, stiffness factor and global damage) (Sadeghi 2011, Sadeghi and Nouban 2016), etc.) up to the failure of column. The concrete confinement due to the transverse reinforcement is also taken into account in RCCAP.

3. Bases of the proposed algorithm

3.1 Division of column into MEs

First, the column is disassembled into two MEs which are located between the inflection point and the critical sections of column (i.e.: maxim moments at the column's two ends). A macro-element (ME) is defined as a fixed-end free-end column subjected to the applied combined loading. Then the responses of MEs are determined and finally, the MEs are assembled to form the column. Identical values of shear force and axial force imposed to inflection point are applied to the ends of the two MEs. By increasing the value of the shear force, the response at the fixed ends of MEs are calculated, while the shear force is increased from zero up to the failure of the member.

For the columns subjected to the combined eccentric axial load, the inflection point is considered at the middle of the column.

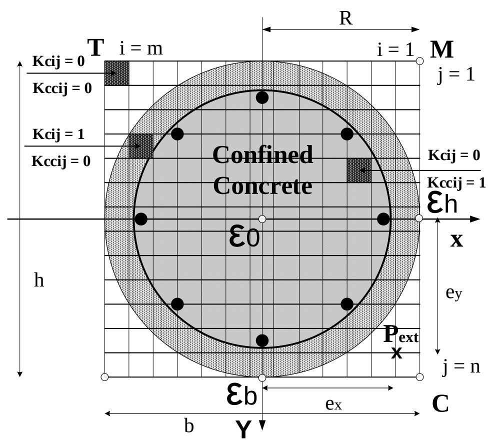

Fig. 2 Discretization of a column's section

3.2 Adapted discretization on sections

The critical sections of RC columns are discretized into FRFEs as shown in Fig. 2.

In the proposed algorithm the FRFEs discretization type with the fixed locations has been applied. This type of discretization, allows the loading-unloading path to be continuously followed up in monotonic and cyclic loading cases. The center of the mesh is positioned on the center of geometry of the cross-section. The external eccentricity orientation angle (θ) is defined as the angle between the external moments' resultant and the y-axis of the section, as illustrated in Fig. 1.

3.3 Application of kinematics Navier's hypothesis

Based on the kinematics Navier's hypothesis it is assumed that the strain distributions at the sections to form a plane, which remains a plane during and after the loading process.

3.4 Constitutive laws applied to materials

3.4.1 Constitutive laws applied to confined and unconfined concretes

Uniaxial constitutive laws are used to simulate the stresses of the concrete elements. To model the behavior of the compressive unconfined and confined concrete elements, the monotonic and cyclic constitutive laws proposed by Sadeghi (2016), and Sadeghi and Nouban (2017) have been used. To simulate the behavior of tensile stress in concrete elements, a linear stress-strain model up to the ultimate tensile strength of concrete is applied. To limit the strains to the maximum values of the compressive strains in unconfined and confined concretes, the formulas proposed by Eurocode 2 (2004) have been used. These formulas are employed to model the loss of concrete cover and the failure of confined concrete.

3.4.2 Constitutive laws applied to reinforcements

To model the behavior of reinforcements, the uniaxial monotonic and cyclic constitutive laws based on Kent-Park's model, similar to those employed by the well-known software such as SAP2000 and ETABS software (CSI, 2008) as well as RUAUMOKO software (Carr, 2017) have been adopted.

3.4.2.1 Monotonic constitutive law applied to reinforcements

The following equations (Eqs. (1) to (7)) have been employed to model the monotonic stress-strain behavior of reinforcements in four phases:

Phase 1 - Linear elastic phase

$$\sigma_s(\varepsilon) = E_s\,\varepsilon \qquad (\text{for } \varepsilon \le \varepsilon_y) \tag{1}$$

Where:

ε_y: The strain at the starting point of the plastic phase (yielding),

E_s: The elasticity modulus of reinforcing steel.

Phase 2 - Plastic plateau phase:

$$\sigma_s(\varepsilon) = F_y \qquad (\text{for } \varepsilon_y < |\varepsilon| \le \varepsilon_{sh}) \tag{2}$$

Where:

ε_{sh}: The strain at the starting point of strain hardening phase,

F_y: The yield strength of reinforcing steel.

Phase 3 - Strain hardening phase:

For this phase, an equation is adopted to find a curve passing two given points having coordinates $A(\varepsilon_0,\ \sigma_{s0})$ and $B(\varepsilon_1,\ \sigma_{s1})$ with two slopes m_0, m_1 as follows

$$\sigma_s = \sigma_{s0} + m_0(\varepsilon - \varepsilon_0) + \mu(\varepsilon - \varepsilon_0)^\beta \tag{3}$$

With

$$\mu = \frac{\sigma_{s1} - \sigma_{s0} - m_0(\varepsilon_1 - \varepsilon_0)}{(\varepsilon_1 - \varepsilon_0)^\beta} \tag{4}$$

$$\beta = \frac{(\varepsilon_1 - \varepsilon_0)(m_1 - m_0)}{\sigma_{s1} - \sigma_{s0} - m_0(\varepsilon_1 - \varepsilon_0)} \tag{5}$$

Therefore, for this phase Eq. (6) can be found and can be used. (CSI 2008, Carr 2017)

$$\sigma_s(\varepsilon) = Sign(\varepsilon)\Big[F_y + E_{sh}(\,|\varepsilon - \varepsilon_{sh}|) - \frac{|\varepsilon - \varepsilon_{sh}|^{(R_1)}}{R_1(\varepsilon_U - \varepsilon_{sh})^{(R_1-1)}}\Big] \tag{6}$$

Where

$$R_1 = \left|\frac{E_{sh}(\varepsilon_U - \varepsilon_{sh})}{F_U - F_y - E_{sh}(\varepsilon_U - \varepsilon_{sh})}\right| \tag{7}$$

And:

F_U: The ultimate strength of reinforcing steel,

ε_{sh}: The strain at the starting point of strain hardening,

ε_U: The strain corresponding to the peak stress

E_{sh}: The slope at the starting point of strain hardening,

Phase 4 - Post-peak phase:

In this phase, after the peak point (ε_U, F_U), elongation increases up to failure without increasing any load.

3.4.2.2 Cyclic constitutive law applied to reinforcements

To model the reinforcement behavior subjected to cyclic loading the constitutive law of Kent-Park which is based on the relationship proposed by Ramberg-Osgood, which considers the Bauschinger effect, have been adopted.

For the loading starting from zero, the monotonic law is applied and unloading from the loading curve follows a path parallel to the initial elastic loading path starting from zero with an inclination of E_r. Thus the unloading path equation will be expressed as follows

$$\sigma_s(\varepsilon) = f_r - E_r\,(\varepsilon_r - \varepsilon) \tag{8}$$

Where:

f_r: Stress at unloading point,

ε_r: Strain at unloading point.

With

$$E_r = E_s \qquad (\text{when } \varepsilon_1 \le \varepsilon_y) \tag{9}$$

$$E_r = E_s\,(21 - \varepsilon_1/\varepsilon_y)/20 \quad (\text{when } \varepsilon_y < \varepsilon_1 \le 4\varepsilon_y) \tag{10}$$

$$E_r = o.85\, E_s \quad \text{(when } \varepsilon_1 > 4\varepsilon_y) \tag{11}$$

Where

$$\varepsilon_1 = |f_r/E_s| \tag{12}$$

And:

E_s: Elasticity modulus of reinforcement.

The unloading curves have the same slope as the slope of the initial elastic loading. Contrary, all following loading after the plastic plateau are nonlinear starting from small stresses due to the Bauschinger effect and are determined from the following equations

$$\varepsilon_s = (\frac{f_s}{E_s})(1 + \left|\frac{f_s}{f_{ch}}\right|^{r-1}) \tag{13}$$

Where

$$f_{ch} = f_y(\frac{0.744}{Ln\,(1+1000\varepsilon_{ip})} - \frac{0.071}{1 - e^{(1000\varepsilon_{ip})}} + 0.241) \tag{14}$$

For the odd loading numbers

$$r = \frac{4.49}{Ln\,(1+n)} - \frac{6.03}{e^n - 1} + 0.297 \quad \text{(for } n = 1, 3, 5, \ldots) \tag{15}$$

For the even loading numbers

$$r = \frac{2.20}{Ln\,(1+n)} - \frac{0.469}{e^n - 1} + 3.04 \quad \text{(for } n=2, 4, 6, \ldots) \tag{16}$$

Where:

ε_s: Strain of reinforcement,

f_s: Stress of reinforcement,

ε_{ip}: Plastic strain of the reinforcement at the precedent loading,

n: Loading number.

The first plastic plateau is achieved for n=0, n=1 corresponds to the first next consecutive loading, n=2 for the second consecutive loading, and so on.

In the model, the buckling in the compression reinforcements is not taken into account. It is assumed that the stirrups prevent the buckling of the reinforcements.

3.5 Strain plane control process

A "strain plane control process" method is adapted in the proposed algorithm to calculate the strains and then the stresses at the centers of the concrete and steel elements. A system of three simultaneous equations with three variables is to be solved by applying a triple iteration process and a proposed difference-based dichotomy convergence numerical search method over the strains. The simultaneous equations are solved to verify the equilibrium state in each section by equating the internal and external efforts. The equilibrium is justified over each section considering the law of "plane sections remain plane during deformation". The solutions are founded considering the cyclic nonlinear behavior of concrete and reinforcement elements. In each concrete element *ij* (*i*, *j*) and in each steel element *k*, the stresses are determined in function of strains (ε). Different loading-unloading stages are determined by means of saving the last three strain values. In order to achieve equilibrium, three characteristic strains comprising ε_C, ε_T and ε_M (as shown in Figs. 1 and 2), are employed as three main variables. Where ε_C represents the strain of the point *C* with the maximum compressive stress in the section, ε_T represents the strain of the point *T* with the maximum tensile stress in the section and finally ε_M represents the strain in the point *M* positioned at a third corner of the section. For non-rectangular section cases the points *C*, *T* and *M* are located out of the structural member section and located on the corners of the discretizing grid.

3.6 Equilibrium state principles

3.6.1 Equilibrium state of sections

The equilibrium state of each section is achieved by equating the internal and external forces and moment

$$P_{ext} = P_{int} \tag{17}$$

$$Mx_{ext} = Mx_{int} \tag{18}$$

$$My_{ext} = My_{int} \tag{19}$$

Where:

P_{ext}: External axial force,

P_{int}: Internal axial force,

Mx_{ext}: External bending moment about the *x*-axis (see Figs. 1 and 2),

My_{ext}: External bending moment about the *y*-axis (see Figs. 1 and 2),

Mx_{int}: Internal bending moment about the *x*-axis,

My_{int}: Internal bending moment about the *y*-axis.

3.6.2 External moments

Eqs. (20) and (21) present the external moments about *x*- and *y*-axis, respectively

$$Mx_{ext} = P_{ext}\,.\,e_y \tag{20}$$

$$My_{ext} = P_{ext}\,.\,e_x \tag{21}$$

Where:

e_x: Eccentricity along the *x*-axis,

e_y: Eccentricity along the *y*-axis.

Eq. (22) presents the external moments' resultant

$$M_{ext} = [(Mx_{ext})^2 + (My_{ext})^2]^{1/2} \tag{22}$$

Eq. (23) presents the orientation angle of the external moments' resultant (or the external eccentricity orientation angle)

$$\theta_{ext} = \theta = Tan^{-1}\,(My_{ext}/Mx_{ext}) \tag{23}$$

It simply can be expressed by Eq. (24) (see Fig. 1), which in this paper, it is called the "external eccentricity orientation angle"

$$\theta_{ext} = \theta = Tan^{-1}\,(e_x/e_y) \tag{24}$$

3.6.3 Internal momens

Eqs. (25) to (28) present the internal efforts

$$P_{int} = \sum_i^m \sum_j^n Kcc_{ij}\,.\,\sigma cc_{ij}\,.\,A_{ij} + \sum_i^m \sum_j^n Kc_{ij}\,.\,\sigma c_{ij}\,.\,A_{ij} \tag{25}$$

$$+\sum_{k}^{ns} \sigma s_k . As_k$$

$$Mx_{int} = \sum_{i}^{m}\sum_{j}^{n} Kcc_{ij} . \sigma cc_{ij} . y_{ij} . A_{ij} + \sum_{i}^{m}\sum_{j}^{n} Kc_{ij} . \sigma c_{ij} . y_{ij} . A_{ij} + \sum_{k}^{ns} \sigma s_k . y_k . As_k \tag{26}$$

$$My_{int} = \sum_{i}^{m}\sum_{j}^{n} Kcc_{ij} . \sigma cc_{ij} . x_{ij} . A_{ij} + \sum_{i}^{m}\sum_{j}^{n} Kc_{ij} . \sigma c_{ij} . x_{ij} . A_{ij} + \sum_{k}^{ns} \sigma s_k . x_k . As_k \tag{27}$$

Eq. (28) presents the internal moments' resultant

$$M_{int} = [(Mx_{int})^2 + (My_{int})^2]^{1/2} \tag{28}$$

Eq. (29) presents the orientation angle of the internal moments' resultant, which in this paper it is called the "internal eccentricity orientation angle"

$$\theta_{int} = Tan^{-1}\,(My_{int}/Mx_{int}) \tag{29}$$

Where:

σcc_{ij}: Stress in confined concrete element *ij*,

σc_{ij}: Stress in unconfined concrete element *ij*,

σs_k: Stress in steel element *k*,

A_{ij}: Area of concrete element *ij*,

As_k: Area of steel element *k*,

Kccij: Material existence indicator for confined concrete element *ij* (*Kccij*=1, indicate the existence of a confined concrete element *ij*),

Kcij: Material existence indicator for unconfined concrete element *ij* (*Kcij*=1, indicate the existence of an unconfined concrete element *ij*),

ns: The number of longitudinal reinforcements in the section,

m: Number of elements in the *y*-direction (equals to the maximum value of *i*),

n: Number of elements in the x-direction (equals to the maximum value of *j*).

Kccij=0 and *Kcij*=0 are employed to indicate a failed element or an imaginary element located out of the section, or in the hollow zone inside the section (Sadeghi 2011) (see Fig. 2).

The equilibrium state is established by finding the resolution of a system with three equations and three variables by means of a triple iteration process and by applying a proposed difference-based dichotomy numerical research method over the characteristic strains.

3.7 Calculation of strains

The strains of the unconfined and confined concrete elements "ε_{ij}" and also the strains of the steel elements "εs_k" are determined as follows

$$\varepsilon_{ij} = \varepsilon_0 + \phi_x(x_{ij} - x_0) + \phi_y(y_{ij} - y_0) \tag{30}$$

$$\varepsilon s_k = \varepsilon_0 + \phi_x(xs_k - x_0) + \phi_y(ys_k - y_0) \tag{31}$$

With:

$$\varepsilon_0 = \varepsilon_C - \phi_x(\mathrm{b}/2) - \phi_y(h/2) \tag{32}$$

Where:

ε_0: Strain at the center of gravity of the section (see Fig. 2),

(x_{ij}, y_{ij}): Coordinates of the center of gravity of concrete element *ij*,

(x_{sk}, y_{sk}): Coordinates of the center of gravity of steel element k,

(x_0, y_0): Coordinates of the center of gravity of the section,

ϕ_x: Curvature in the *x*-direction,

ϕ_y: Curvature in the *y*-direction.

3.8 Calculation of curvatures

The values of the curvatures in the *x* and *y* directions are determined by employing the following equations

$$\phi_x = \frac{(\varepsilon_h - \varepsilon_0)}{(b/2)} \tag{33}$$

$$\phi_y = \frac{(\varepsilon_b - \varepsilon_0)}{(h/2)} \tag{34}$$

With

$$\varepsilon_h = \frac{\varepsilon_C + \varepsilon_M}{2} \tag{35}$$

$$\varepsilon_b = \varepsilon_C + \frac{\varepsilon_T}{2} - \frac{\varepsilon_M}{2} \tag{36}$$

The *b* and *h* dimensions, as well as the locations of ε_b and ε_h, are illustrated in Fig. 2.

The overall curvature "ϕ" is given as

$$\phi = \sqrt{{\phi_x}^2 + {\phi_y}^2} \tag{37}$$

3.9 ME loading history recording

Every loading step is saved and is compared to the two preceding steps.

For every loading step p, on each critical section $\boldsymbol{l}$, for the imposed force (moment) "$M_{ext}(p, l)$", the difference factors "$dM1$ and $dM2$" are calculated. The difference factors indicate the loading cases.

$$dM1 = M_{ext}(p-1, l) - M_{ext}(p-2, l) \tag{38}$$

$$dM2 = M_{ext}(p, l) - M_{ext}(p-1, l) \tag{39}$$

Loading cases are identified as follows:

• It is a loading case if

$$[dM1 \geq 0 \text{ and } dM2 > 0] \tag{40}$$

• It is an unloading just after a loading case if

$$[dM1 \geq 0 \text{ and } dM2 < 0] \tag{41}$$

• It is an unloading after an unloading case if

$$[dM1 < 0 \text{ and } dM2 < 0] \tag{42}$$

• It is a reloading after unloading case if

$$[dM1 < 0 \text{ and } dM2 > 0] \quad (43)$$

3.10 Recording the concrete elements loading history

The three last stress and strain values for each concrete element *ij* are saved and compared. For every concrete element *ij* discretized on section l, in the step *p* of loading, the difference factors "$d\varepsilon 1$ and $d\varepsilon 2$" are calculated.

$$d\varepsilon 1 = \varepsilon(p-1, l, i, j) - \varepsilon(p-2, l, i, j) \quad (44)$$

$$d\varepsilon 2 = \varepsilon(p, l, i, j) - \varepsilon(p-1, l, i, j) \quad (45)$$

The loading cases on the strain-stress curve of each concrete element are identified by the following conditions:

- It is a loading case if

$$[d\varepsilon 1 \geq 0 \text{ and } d\varepsilon 2 > 0] \quad (46)$$

- It is an unloading just after a loading case if

$$[d\varepsilon 1 \geq 0 \text{ and } d\varepsilon 2 < 0] \quad (47)$$

- It is an unloading after an unloading case if

$$[d\varepsilon 1 < 0 \text{ and } d\varepsilon 2 < 0] \quad (48)$$

- It is a reloading after unloading case if

$$[d\varepsilon 1 < 0 \text{ and } d\varepsilon 2 > 0] \quad (49)$$

3.11 Recording the steel elements loading history

The three last stress and strain values for each steel element *k* are saved and compared. For every steel element k discretized on section l, in the step p of loading, the difference factors "$d\varepsilon 1$ and $d\varepsilon 2$" are calculated.

$$d\varepsilon 1 = \varepsilon(p-1, l, k) - \varepsilon(p-2, l, k) \quad (50)$$

$$d\varepsilon 2 = \varepsilon(p, l, k) - \varepsilon(p-1, l, k) \quad (51)$$

The loading cases on the strain-stress curve of each steel element are identified by the following four different typical cases as defined below:

- It is a loading case if

$$[d\varepsilon 1 \geq 0 \text{ and } d\varepsilon 2 > 0] \quad (52)$$

- It is an unloading just after a loading case if

$$[d\varepsilon 1 \geq 0 \text{ and } d\varepsilon 2 < 0] \quad (53)$$

- It is an unloading after an unloading case if

$$[d\varepsilon 1 < 0 \text{ and } d\varepsilon 2 < 0] \quad (54)$$

- It is a reloading after unloading case if

$$[d\varepsilon 1 < 0 \text{ and } d\varepsilon 2 > 0] \quad (55)$$

3.12 Proposed strain-based design (SBD) method

The strain-based design (SBD) method is defined and proposed by the authors due to the following reason: firstly the maximum strain in concrete on the most compressive point on the section (ε_c) can be limited to the ultimate design strain for concrete (i.e.: $\varepsilon_c \leq 0.003$ according to ACI-318-14) and secondly by changing ε_c, the equilibrium in the critical section can be achieved for any targeted force or targeted displacement and also ε_c can be increased to find the pushover curve or by increasing and decreasing ε_c, the hysteretic curve can be produced up to the failure of the column.

ε_c as a key sensitive strain at point *C* at the most compressed point acts as an indicator for following up the trajectory of loading-unloading paths and it can be used for any case of loading. Actually ε_c is used to navigate the loading path in the simulation of the response of the column.

During application of loading history on the column, the three last stress and strain values for the point *C* (the most compressive stress point on the critical section of the column) are saved and compared. For the point *C* situated at the corner of the critical section, in the step p of loading, the difference factors "$d\varepsilon c1$ and $d\varepsilon c2$" are calculated.

$$d\varepsilon c1 = \varepsilon c(p-1) - \varepsilon c(p-2) \quad (56)$$

$$d\varepsilon c2 = \varepsilon c(p) - \varepsilon c(p-1) \quad (57)$$

The loading cases are identified by the following conditions:

- It is a loading case i

$$[d\varepsilon c1 \geq 0 \text{ and } d\varepsilon c2 > 0] \quad (58)$$

- It is an unloading just after a loading case if

$$[d\varepsilon c1 \geq 0 \text{ and } d\varepsilon c2 < 0] \quad (59)$$

- It is an unloading after an unloading case if

$$[d\varepsilon c1 < 0 \text{ and } d\varepsilon c2 < 0] \quad (60)$$

- It is a reloading after unloading case if

$$[d\varepsilon c1 < 0 \text{ and } d\varepsilon c2 > 0] \quad (61)$$

These load cases match directly by the load cases applied on the ME and entire column.

3.13 Proposed triple simultaneous dichotomy convergence method

A proposed triple simultaneous dichotomy iteration method is applied to find the equilibrium state in each section of the column that repeatedly for three different sets of strains bisects the intervals and then selects the subinterval in which the roots must lie for further processing. The method is applicable to solve numerically the equation $F(\varepsilon)$=0 for the variable ε, where F is a continuous function defined on an interval $[\varepsilon_1, \varepsilon_2]$. The interval $[\varepsilon_1, \varepsilon_2]$ for the section's equilibrium state search are $[(\varepsilon_{Cmin}, \varepsilon_{Cmax}]$, $[\varepsilon_{Tmin}, \varepsilon_{Tmax}]$ and $[(\varepsilon_{Mmin}, \varepsilon_{Mmax}]$, respectively.

The strain of the most compressive point (point C) (see Figs. 1 and 2)

$$\varepsilon_C = (\varepsilon_{Cmin} + \varepsilon_{Cmax})/2 \quad (62)$$

The strain of the most tensile point (point T) (see Figs. 1 and 2)

$$\varepsilon_T = (\varepsilon_{Tmin} + \varepsilon_{Tmax})/2 \quad (63)$$

The strain in the point M positioned at the third corner of the section (see Figs. 1 and 2)

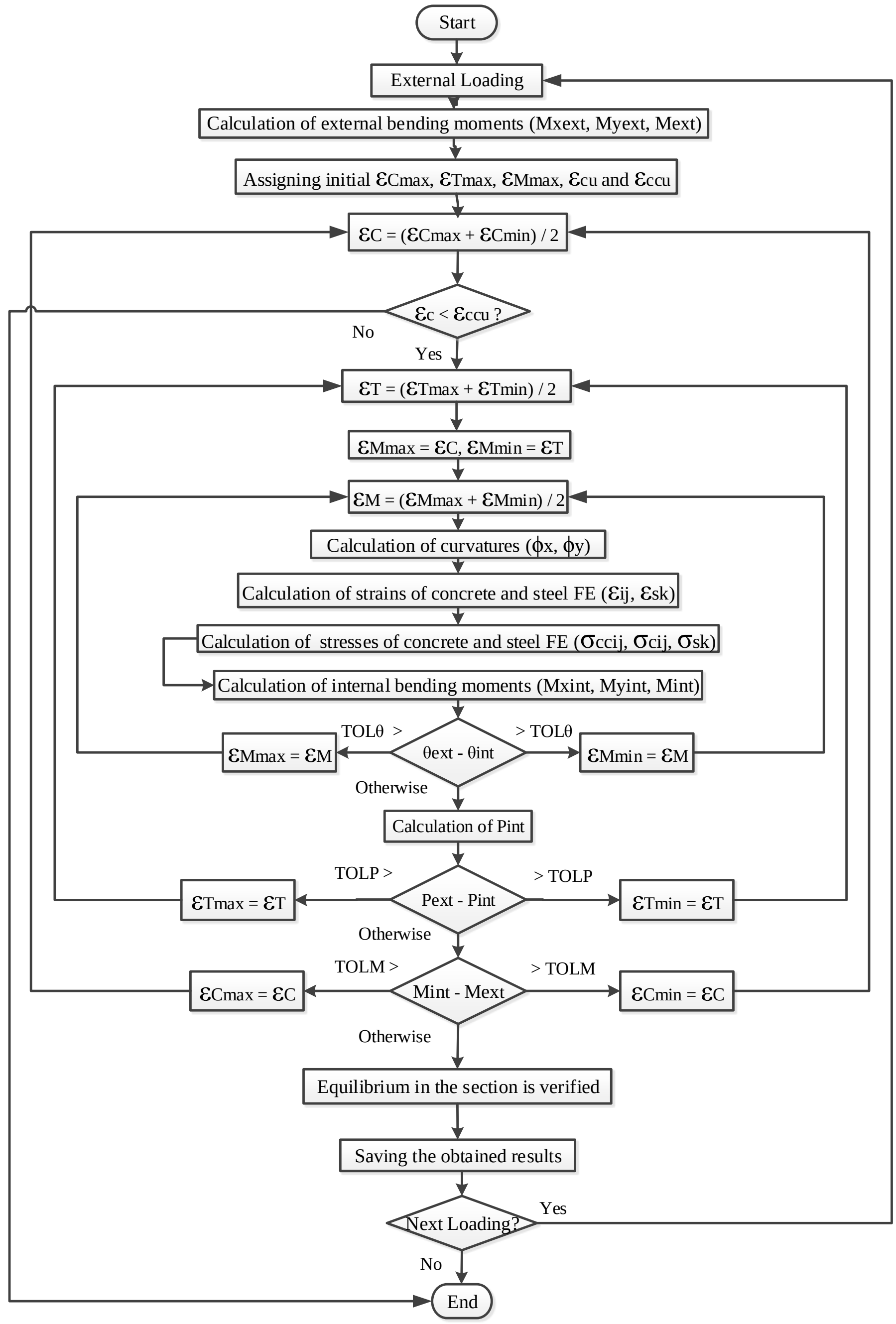

Fig. 3 Proposed convergence procedure to approach the equilibrium state in a section of the column

$$\varepsilon_M = (\varepsilon_{Mmin} + \varepsilon_{Mmax})/2 \quad (64)$$

The initial values for ε_{Mmin} and ε_{Mmax} can be considered as ε_T and ε_C, respectively.

In loading or reloading cases

$$\varepsilon_T \leq \varepsilon_M \leq \varepsilon_C \quad (65)$$

In unloading cases

$$\varepsilon_T \geq \varepsilon_M \geq \varepsilon_C \quad (66)$$

3.14 Equilibrium state verification

To achieve the equilibrium state, a set of successive iteration processes is followed up to satisfy the following three conditions:

3.14.1 Eccentricity orientation angle verification

The external eccentricity orientation angle θ (as illustrated in Fig. 1) and the internal eccentricity orientation angle must be balanced. This is tested by applying an iteration process over the strain of point M (ε_M) for the given value of ε_C and ε_T as demonstrated in the flowchart given in Fig. 3.

In the trial process, an average strain value is employed, as given by the following equation

$$\varepsilon_{M(i+1)} = (\varepsilon_{Mmin\,(i)} + \varepsilon_{Mmax\,(i)})/2 \quad (67)$$

In the proposed algorithm for the eccentricity orientation angle, the reasonably accurate convergence tolerance given below is employed for verification of the equilibrium state. Therefore the following condition must be satisfied for the eccentricity orientation angle:

$$|\theta_{ext} - \theta_{int}| \leq 0.1° \quad (68)$$

3.14.2 Verification of axial forces

By applying a second iteration process over the extreme tensile strain at point T (ε_T) for the given value of ε_C, the equilibrium between the internal axial and external forces is confirmed as illustrated in the flowchart given in Fig. 3.

The average strain value is employed in the following next trial

$$\varepsilon_{T(i+1)} = (\varepsilon_{Tmin\,(i)} + \varepsilon_{Tmax\,(i)})/2 \quad (69)$$

In the proposed algorithm for the axial force, the reasonably accurate convergence tolerance given below is employed to verify the equilibrium state. Therefore the following condition must be satisfied for the axial force

$$|P_{ext} - P_{int}| \leq 0.001\,|P_{ext}| \quad (70)$$

3.14.3 Verification of bending moments

By applying a third iteration process over the extreme compressive strain (in point *C*), the equilibrium between the internal and external bending moments is verified as shown in the flowchart in Fig. 3.

The average strain value is employed in the following trial

$$\varepsilon_{C(i+1)} = (\varepsilon_{Cmin\,(i)} + \varepsilon_{Cmax\,(i)})/2 \quad (71)$$

In the proposed algorithm for the bending moment, the reasonably accurate convergence tolerance given below is employed for verifying the equilibrium state. Therefore the following condition must be satisfied for the bending moment

$$|M_{ext} - M_{int}| \leq 0.001\,|M_{ext}| \quad (72)$$

3.15 Convergence procedure to achieve the equilibrium state in a section

3.15.1 Applied proposed dichotomy convergence method

A proposed triple simultaneous dichotomy convergence method is applied as a root-finding process that continually bisects an interval and accordingly chooses a subinterval in which a root must lie for further processing.

The method is appropriate to find the numerical solution of the equation $F(\varepsilon) = 0$ for the variable ε, where *f* is a function defined on an interval $[\varepsilon_1, \varepsilon_2]$ which are said to bracket a root. The proposed dichotomy method is a difference-based method.

At each step, the midpoint $\varepsilon_3 = (\varepsilon_1+\varepsilon_2)/2$ of the interval and the value of the function $F(\varepsilon_3)$ at that point are computed. The method chooses the subinterval that is assured to be a bracket as the new interval to be employed in the succeeding step. The process is continued until the interval is sufficiently small or the desired accuracy tolerances achieved.

The input for the method is a function *f*, an interval $[\varepsilon_1, \varepsilon_2]$, and the function values $F(\varepsilon_1)$ and $F(\varepsilon_2)$. Each iteration performs the following steps:

1. Calculation of $\varepsilon_3 = (\varepsilon_1 + \varepsilon_2)/2$, the midpoint of the interval.
2. Calculation of the function value ($F(\varepsilon_3)$) at the midpoint.
3. If the convergence criterion is satisfied (that is, ε_3-ε_1 is adequately small, or $|F(\varepsilon_3)|$ is adequately small), returning the ε_3 and stopping the iterating.
4. Comparing the $F(\varepsilon_3)$ value with the acceptable accuracy tolerances and replacing either (ε_1, $F(\varepsilon_1)$) or (ε_2, $F(\varepsilon_2)$) with (ε_3, $F(\varepsilon_3)$) so that there is a new ε_3 within the new interval.

During the implementation of the method on the computer program, there are problems with finite accuracy, so there are convergence acceptance tolerance limits of the function under question. Moreover, the difference between ε_1 and ε_2 is limited by the floating point accuracy; i.e., as the difference between ε_1 and ε_2 decreases, at some point, the midpoint of $[\varepsilon_1, \varepsilon_2]$ will be numerically identical to (within floating point precision of) either ε_1 or ε_2.

In the proposed algorithm, the method is written in pseudocode and for the three loops of iteration processes the following variables, functions, and tolerances are adapted:

The input of loop 1:
  Function *f*: $\theta_{ext} - \theta_{int}$,
  Endpoint values ε_1, ε_2: $\varepsilon_{M\min}$, ε_{Mmax},
  Tolerance (TOLθ): 0.1°.
The output of loop 1:
  The value that differs from a root of θ (ε) = 0 by less than TOLθ.
The input of loop 2:
  Function *g*: $P_{ext} - P_{int}$,
  Endpoint values ε_1, ε_2: ε_{Tmin}, ε_{Tmax},
  Tolerance (TOLP): $0.001\,|P_{ext}|$.
The output of loop 2:
  The value that differs from a root of $P(\varepsilon)$=0 by less than TOLP.
The input of loop 3:
  Function *h*: $M_{ext} - M_{int}$,
  Endpoint values ε_1, ε_2: $\varepsilon_{C\min}$, $\varepsilon_{C\max}$,
  Tolerance (TOLM): $0.001\,|M_{ext}|$.
The output of loop 3:
The value that differs from a root of $M(\varepsilon)$=0 by less than TOLM.

Note that the functions *f*, *g*, and *h* are functions of stress (σ), but since the stress (σ) of each concrete or steel element is a function of its strain (ε), the functions *f*, *g*, and *h* are considered as functions of strain (ε).

3.15.2 Flowchart of convergence procedure

Fig. 3 presents the flow chart for the part of the convergence procedure to achieve the equilibrium state in a section of the column.

3.16 Determination of displacements

The elastic-plastic method (EPM) proposed by Priestley *et al*. (2007) is adapted in RCCAP to calculate the displacements. The EPM reflects the fact that the columns are vastly affected in the critical zone when they are subjected to eccentric axial force or lateral loading. The main effect on the rotation and deflection of the column is due to the curvature registered at critical sections. The loading followed the peak value on the M-ϕ curve at the critical section, a significant local change occurs at the critical section where a pseudo-plastic hinge forms. After passing the peak, the curvature development is mostly due to the plastic hinge formed in the critical zone. Whereas in the other regions, the cracks are closed and the curvatures decrease quickly to close zero. The plastic hinge length of columns is a critical demand parameter in the nonlinear analysis of structures using the finite element method. The numerical model of a plastic hinge plays an important role in evaluating the response and damage of a structure subjected to earthquakes or other loads causing the formation of plastic hinges. The existing researches demonstrate that the plastic hinge length of RC columns mainly depends on the section size, reinforcement ratio, reinforcement strength, concrete strength, and axial compression value (Tang *et al*. 2016).

The EPM is applied for two phases of before and after appearing a pseudoplastic hinge in the critical section of the column by employing Eqs. (73) and (74), respectively.

$$\delta = \left(\frac{\phi}{3}\ L^2\right) \quad \text{(for } \phi \le \phi_p\text{)} \tag{73}$$

$$\delta = \left(\frac{\phi_p}{3}\ L^2\right) + (\phi - \phi_p)(L_p)(L - 0.5\ L_p) \quad \text{(for } \phi \ge \phi_p\text{)} \tag{74}$$

Where:

δ: Relative displacement at the end of ME,
ϕ: Curvature at the critical section,
ϕ_p: Curvature when a plastic hinge is formed,
L: Length of ME,
L_p: Length of the plastic hinge.

4. Experimental test data

The experimental tests performed by Garcia Gonzalez (1990), Park (1989) have been used to verify the proposed algorithm. The Garcia Gonzalez tests were performed on several columns under cyclic eccentric loading (CEL), and monotonic eccentric loading (MEL). The characteristics of the tested physical model are summarized as follows: dimensions of rectangular section=18 cm×25 cm, column height=1.75 m, percentage of steel ρ=1%, the concrete of strength f_c'=42 MPa, stirrups of 6 mm diameter with 9 cm spacing, the yield strength of reinforcing steels: F_y=470 MPa. The columns were fixed at the bottom, free at the top. The tests were performed for different angles of applied external moments' resultant (θ). The columns were simultaneously under a 500 kN vertical loading and a lateral displacement applied to the top of the column. In this paper, the experimentally tested model is called "reference model" and its critical section is called "reference section".

Park performed a test on a rectangular RC column under cyclic combined loading. They tested a column subjected to cyclic monoaxial bending moment and a compression axial loading of 160 kN, having a section of 30.5 cm×15.2 cm with four longitudinal reinforcement of type mild steel with a yield strength of 345 MPa and steel percentage of ρ=2.4%. The used concrete had a compression ultimate stress of 34 MPa.

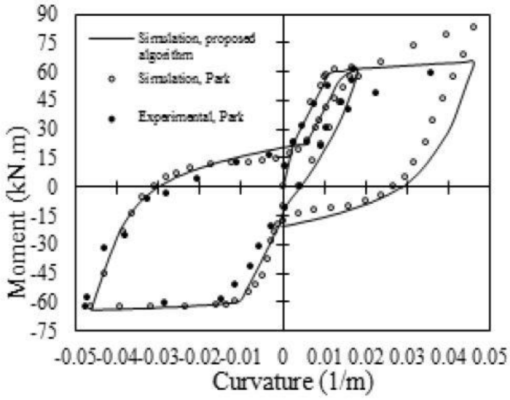

Fig. 4 The M-ϕ response, cyclic combined loading case

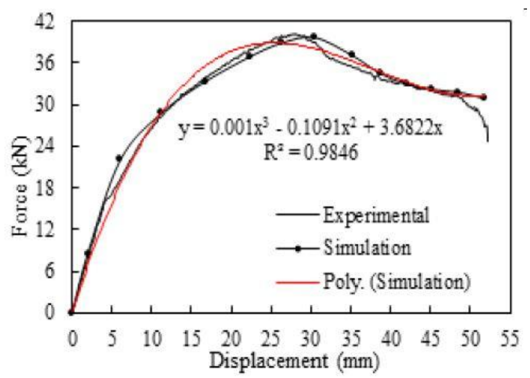

Fig. 5 Force-displacement response of the reference model, MEL, θ= 0°

5. Verification of the proposed algorithm

Figs. 4 to 7 demonstrate the comparison of the results obtained from the numerical simulation applying the proposed algorithm and the experimental test results. As can be seen from these figures, there is a close agreement between the simulation results using the proposed algorithm and the experimental test results.

In Fig. 4, the results obtained from the simulation applying the proposed algorithm and the simulation/experimental test performed by Park *et al*. on an RC column subjected to cyclic combined loading are compared.

Fig. 5, shows the comparison of the results obtained from the proposed simulation and the experimental test of Garcia Gonzalez (1990) on the reference model under MEL with the eccentricity orientation angle (θ) of 45°.

As depicted in Fig. 5, the polynomial degree 3 trendline

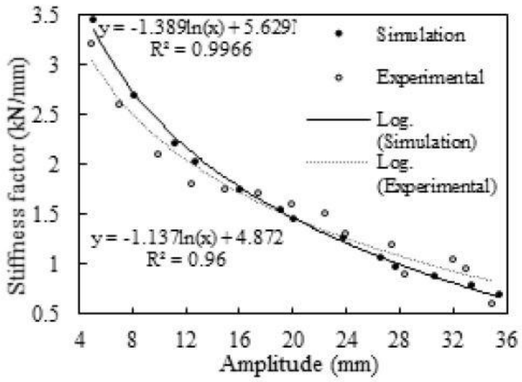

Fig. 6 Stiffness factor, CEL, θ=30°

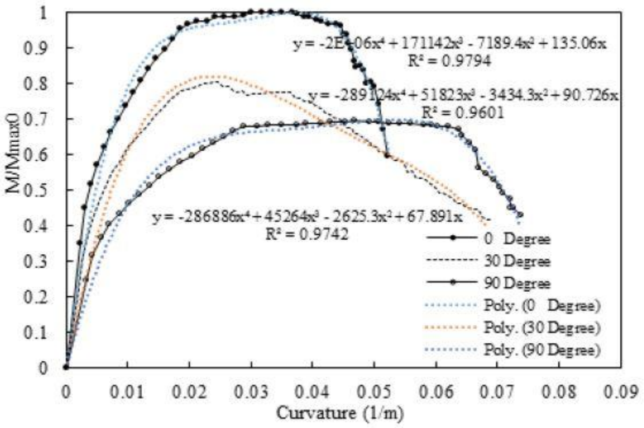

Fig. 7 M-ϕ response of the reference section, MEL, different θ

type matches very well with the variation of the simulated force-displacement response curve. For the reference column under MEL, the simulation shows the relation give in Eq. (75) with a determination factor of R^2=0.9846 for the eccentricity orientation angle of $\theta = 0°$.

$$F = 0.001\delta^3 - 0.1091\delta^2 + 3.6822\,\delta \tag{75}$$

In Eq. (75), F and δ are expressed in kN and in mm, respectively.

In Fig. 6, the results obtained applying the proposed algorithm are compared to the results of the experimental test of Garcia Gonzalez (1990) for the stiffness factor for CEL at maximum positive displacement at each loop of the hysteretic curve.

As illustrated in Fig. 6, the logarithmic trendline type matches very well with the variation of the stiffness factor. For the reference columns under CEL the simulation shows the relation give in Eq. (76) with a determination factor of R^2=0.9966 and the experimental test indicate the relation given in Eq. (77) with R^2=0.96 for the stiffness factor for the eccentricity orientation angle of $\theta = 30°$.

$$K = -1.389\ln(a) + 5.6291 \tag{76}$$

$$K = -1.137\ln(a) + 4.872 \tag{77}$$

Where:
K: Stiffness factor at each amplitude in kN/mm,
a: Amplitude in mm.

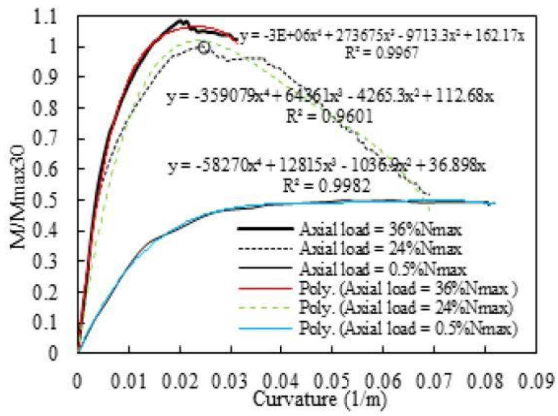

Fig. 8 Influence of axial force on the response of the reference section, MEL, θ=30°

Two examples showing the influence of eccentricity orientation angle and axial force on the behavior of the columns are presented in Figs. 7 and 8.

Fig. 7 illustrates the normalized bending moment (Moment/Mmax0) versus curvature of the critical section of the reference model for different eccentricity orientation angles (θ) of 0°, 30° and 90° and the axial load of 500 kN. Where Mmax0 represents the ultimate resisting moment about the main axis of the section (when θ=0°). As can be seen from this figure, the post-elastic stiffness as well as the ultimate strength of the section decrease with the increase in the value of the external eccentricity orientation angle (θ). In the cases of eccentricity orientation angles of 30° and 90°, compared to the case of the eccentricity orientation angle of 0°, the decrease of the ultimate strength is about 20% and 32%, respectively.

As demonstrated in Fig. 7, the polynomial degree 4 trendline type matches very well with the variation of the simulated moment-curvature (M-ϕ) response curves for different values of θ. For the reference column under MEL, the simulation shows the relations of the M-ϕ response give in Eqs. (78) to (80) with the determination factors of R^2=0.9794, R^2=0.9601 and R^2=0.9742 for the eccentricity orientation angles of $\theta = 0°, 30°$ and 90°, respectively. In Eqs. (78), (79), (80), (81), (82) and (83), the curvature (ϕ) is expressed in 1/m.

$$M/M_{max\,0} = -2\times10^6\phi^4 + 171142\phi^3 - 7189.4\phi^2 + 135.06\phi \tag{78}$$

$$M/M_{max\,0} = -289124\phi^4 + 51823\phi^3 - 3434.3\phi^2 + 90.726\phi \tag{79}$$

$$M/M_{max\,0} = -286886\phi^4 + 45264\phi^3 - 2625.3\phi^2 + 67.891\phi \tag{80}$$

Fig. 8 demonstrates the normalized bending moment versus curvature for the critical section of the reference model subjected to different applied axial force values in the case for an eccentricity orientation angle of θ=30°. Where M_{max30} represents the resisting moment of the section when θ=30°. As Fig. 8 indicates, the ultimate strength and stiffness of the column increase when the axial force

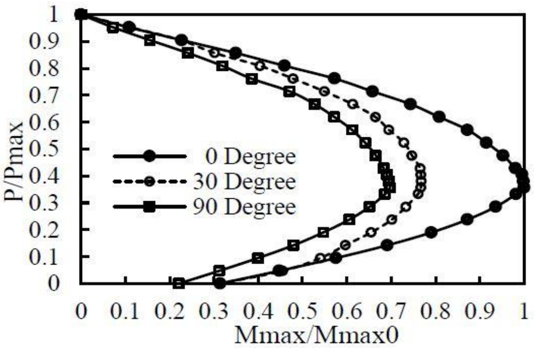

Fig. 9 Interaction diagram of reference section, MEL, θ of 0°, 30° and 90°

increases, and also the failure occurs earlier. Large axial loads, make the column brittle, impose a large material loss and reduce the ductility. Therefore, these items must be considered carefully in the design of prestressed members, because the axial force initiates an action of the type "prestressed". By the same token, the design of structures in high-risk seismic zones must be carried out with great care due to the added axial loads.

As shown in Fig. 8, the polynomial degree 4 trendline type matches very well with the variation of the simulated moment-curvature response curves for various values of normalized axial force ratio (P/P_{max}). For the reference column under MEL, the simulation shows the relations of the M-ϕ response give in Eqs. (81) to (83) with the determination factors of R^2=0.9967, R^2=0.9601 and R^2=0.9982 for the values of P/P_{max} equals to 36%, 24% and 0.5%, respectively when θ=30°:

$$M/M_{max\,30} = -3\times10^6\phi^4 + 273675\phi^3 - 9713.3\phi^2 + 162.17\phi \tag{81}$$

$$M/M_{max\,30} = -359079\phi^4 + 64361\phi^3 - 4265.3\phi^2 + 112.68\phi \tag{82}$$

$$M/M_{max\,30} = -58270\phi^4 + 12815\phi^3 - 1036.9\phi^2 + 36.898\phi \tag{83}$$

6. Interaction diagram

Fig. 9 illustrates the normalized axial force-bending moment interaction diagram of the reference section for eccentricity orientation angles (θ) of 0°, 30° and 90°. The ultimate resisting moments of the section (M_{max}) are normalized to the maximum ultimate resisting moment of the section when θ=0° (M_{max0}). This figure illustrates that in the reference section, for all eccentricity orientation angles, the balance point occurs when the applied axial force (P) is about 38% of Pmax. At the balance point, the increase of the ultimate resisting moment is about 320%, 245% and 315% compared to the case of no axial load is applied for the eccentricity orientation angles of 0°, 30° and 90°., respectively. Based on the calculation performed, it was

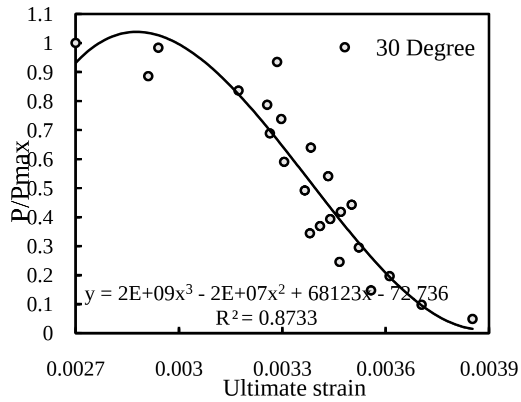

Fig. 10 Ultimate strain at extreme compression fiber "ε_u", MEL

observed that the minimum enhancement of the ultimate strength of the section due to the axial force is observed when the eccentricity orientation angle matches with the direction of the diagonal of the section (i.e., when θ=Tan^{-1} (h/b)=36°).

7. Assessment of ultimate strain (ε_u)

In Fig. 10, the evolution of ultimate strain at extreme compression fiber ε_u (at the corner C) of a rectangular RC section due to the ultimate moment versus applied normalized axial force (P/P_{max}) for the eccentricity orientation angle of 30° is shown. As the obtained results and their adapted trendlines show, the ultimate strain decreases with increasing the axial force and it generally, ranges from 0.0027 to 0.0039. Therefore, the 0.003 value given by ACI-318-14 code for the ultimate strain in the design in extreme compression fiber of the section, is not conservative and valid for the combined load cases with large axial force.

As shown in Fig. 10, the polynomial degree 3 trendline type matches well with the variation of the simulated ultimate strains at extreme compression fiber of the section "ε_u" in case of MEL for different values of values P/P_{max}. For the reference column under MEL, the simulation shows the relation give in Eq. (84) with the determination factor of R^2=0.8733 for the values of P/P_{max} when θ=30°.

$$P/P_{max} = 2\times10^9{\varepsilon_u}^3 - 2\times10^7{\varepsilon_u}^2 + 162.17\varepsilon_u - 72.736 \tag{84}$$

8. Conclusions

An algorithm for simulation of monotonic or cyclic eccentrically-loaded RC columns using fixed rectangular finite elements discretization together with a finite element computer program has been submitted. The proposed simulation algorithm has been validated by experimental test data. The interaction diagrams for rectangular sections under different eccentric axial loads with different eccentricity orientation angles indicate that the increase in the axial force, increases the strength of column up to the "balance point" for any eccentricity orientation angle at approximately the same value of the axial load. With the increase of the axial force, the ultimate strength and stiffness of the member increase, but large axial loads reduce the ductility of the columns, make them brittle, impose great loss of material, and cause the early failure of the RC columns. Therefore, these items must be considered carefully in the design of prestressed members, and also in the design of RC structures in high-risk seismic zones due to the added axial loads to the RC columns.

The study of the ultimate strain at extreme compression fiber of a rectangular RC section for different eccentricity orientation angles shows that the ultimate strain decreases with increasing the axial force. The results of the examined cases show that the 0.003 value given by ACI-318 code for ultimate strain, is not conservative and valid for the combined load cases with large axial force.

Acknowledgments

The support of the Ecole Centrale de Nantes/France and the Near East University/Cyprus is appreciated.

References

Abd El Fattah A.M., Rasheed, H.A. and Al-Rahmani, A.H. (2017), "Partial confinement utilization for rectangular concrete columns subjected to biaxial bending and axial compression", *Int. J. Concrete Struct. Mater.*, **11**(1), 135-149.

Amziane, S. and Dubé, J.F. (2008), "Global RC structural damage index based on the assessment of local material damage", *J. Adv. Concrete Technol.*, **6** (3), 459-468.

Carr, A.J. (2017), "Ruaumoko theory manual", Technical Report, Volume 1: Theory, University of Canterbury, Carr Research, New Zealand.

CSI (2008), Material Stress-Strain Curves, Technical Note, Computers and Structures, Inc., California, USA.

Elwan, S.K. and Omar, M.A. (2014), "Experimental behavior of eccentrically loaded RC slender columns strengthened using GFRP wrapping", *Steel Compos. Struct.*, **17**(3), 271-285.

Eurocode 2 (2004) Design of Concrete Structures-Part 1-1: General Rules and Rules for Buildings, European Standard (Norme Europeenne), ICS 91.010.30; 91.080.40, EN 1992-1-1 (English Version), The European Union per Regulation 305/2011, Directive 2004/18/EC.

Garcia Gonzalez, J.J. (1990), "Contribution á l'étude des poteaux en béton armé soumis á un cisaillement dévié alterné", Ph.D. Dissertation, University of Nantes/Ecole Centrale de Nantes, Nantes.

Kang, J.W. and Lee, J. (2018), "A correction method for objective seismic damage index of reinforced concrete columns", *Comput. Concrete*, **21**(6), 741-748.

Massumi, A. and Badkoubeh, A.R. (2015), "Dimensionless analysis of composite rectangular and circular RC columns", *Steel Compos. Struct.*, **19**(2), 327-348.

Nigdeli, S.M., Bekdaş, G., Kim, S. and Geem, Z.W. (2015), "A novel harmony search-based optimization of reinforced concrete biaxially loaded columns", *Struct. Eng. Mech.*, **54**(6), 1097-1109.

Park, R. (1989), "Evaluation of ductility of structures and structural assemblages from laboratory testing", *Bull. NZ Nat. Soc. Earthq. Eng.*, **22**(3), 155-166.

Peng, Ch. and Guner, S. (2018), "Direct displacement-based seismic assessment of concrete frames", *Comput. Concrete*, **21**(4), 355-365.

Pires, S.L. and Silva Maria, C.A.T. (2014), "A numerical procedure for reinforced concrete columns with a focus on stability analysis", *Comput. Concrete*, **14**(6), 657-674.

Priestley, M.J.N., Calvi, M.C. and Kowalsky, M.J. (2007), "Displacement-based seismic design of structures", Istituto Universitario di Studi Superiori di Pavia, IUSS Press, Pavia.

Rodrigues, E.A., Manzoli, O.L., Bitencourt, Jr. L.A.G., dos Prazeres, P.G.C. and Bittencourt, T.N. (2015), "Failure behavior modeling of slender reinforced concrete columns subjected to eccentric load", *Lat. Am. J. Solid. Struct.*, **12**(3), 520-541.

Sadeghi, K. (2011), "Energy based structural damage index based on nonlinear numerical simulation of structures subjected to oriented lateral cyclic loading", *Int. J. Civil Eng.*, **9**(3), 155-164.

Sadeghi, K. (2016), "Nonlinear-static oriented pushover analysis of reinforced concrete columns using variable oblique finite elements discretization", *Int. J. Civil Eng.*, **14**(5), 295-306.

Sadeghi, K. and Nouban, F. (2016), "Damage quantification and fatigue of RC structures", *Struct. Eng. Mech.*, **58**(6), 1021-1044.

Sadeghi, K. and Nouban, F. (2017), "Behavior modeling and damage quantification of confined concrete under cyclic loading", *Struct. Eng. Mech.*, **61**(5), 625-635.

Shirmohammadi, F. and Esmaeily, A. (2016), "Software for biaxial cyclic analysis of reinforced concrete columns", *Comput. Concrete*, **17**(3), 353-386.

Szerszen, M.M., Szwed, A. and Nowak, A.S. (2005), "Reliability analysis for eccentrically loaded columns", *ACI Struct. J.*, **102**(5), 676-688.

Tang, Z., Ma, H., Guo, J., Xie, Y. and Li, Z. (2016), "Experimental research on the propagation of plastic hinge length for multi-scale reinforced concrete columns under cyclic loading", *Earthq. Struct.*, **11**(5), 823-840.

CC